AIP | Review of Scientific Instruments

Plasma ion source for in situ ion bombardment in a soft x-ray magnetic scattering diffractometer

Daniel Lengemann, Dieter Engel, and Arno Ehresmann

Citation: Review of Scientific Instruments **83**, 053303 (2012); doi: 10.1063/1.4718937
View online: http://dx.doi.org/10.1063/1.4718937
View Table of Contents: http://scitation.aip.org/content/aip/journal/rsi/83/5?ver=pdfcov
Published by the AIP Publishing

Plasma ion source for *in situ* ion bombardment in a soft x-ray magnetic scattering diffractometer

Daniel Lengemann,[a] Dieter Engel, and Arno Ehresmann
Institute of Physics, EP IV, University of Kassel, Heinrich-Plett-Str.40, 34132 Kassel, Germany and Center for Interdisciplinary Nanostructure Science and Technology (CINSaT), University of Kassel, Heinrich-Plett-Str.40, 34132 Kassel, Germany

(Received 16 March 2012; accepted 2 May 2012; published online 23 May 2012)

A new plasma ion source for *in situ* keV He ion bombardment of solid state samples or thin films was designed and built for ion fluences between 1×10^{12} and 1×10^{17} ions/cm^2. The system was designed to be mounted to different diffraction chambers for soft x-ray resonant magnetic scattering. Without breaking the vacuum due to He-ion bombardment, structural and magnetic modifications of the samples can be studied *in situ* and element specifically. © *2012 American Institute of Physics*. [http://dx.doi.org/10.1063/1.4718937]

I. INTRODUCTION

The preparation of thin films, and the deliberate modification of their characteristics during or after deposition, is the basis for a multitude of technological applications, in particular, in data storage or sensor devices. Whereas thin films can be deposited by a multitude of techniques, there are only a few techniques to modify layer characteristics after deposition. Among these *a posteriori* methods, the bombardment of thin films with ion projectiles is the most versatile. Surface topographies may be tailored by focussed heavy ion beam milling or heavy ion bombardment induced ripple formation.[1] Electrical or magnetic characteristics may be changed, when heavy ions are implanted,[2] or they may be used to create defects and thereby change the structure of the thin film system.[3] When using heavy ions to modify thin film systems, however, applied fluences have to be rather low since otherwise, high sputter yields would destroy the film. Light ions (H^+, He^+) in the 10 keV kinetic energy regime, on the other hand, can be used up to medium fluences with almost no sputter effects (sputter yields of He^+ ions are at least one order of magnitude lower than for other noble gases[4]). Particularly, keV He^+ ion bombardment is of scientific and technological interest since it has been used in the closer past, e.g., to induce chemical order,[5] or magnetic phase transitions,[6] to create artificial domains,[7,8] or to tailor magnetic anisotropies.[9] Moreover, He^+ ions will not change the chemical composition of the layer system, but will induce a relatively small density of defects and deposit energy into the thin film system.

Therefore, the characterization of structure or element specific magnetic/electric modifications is usually difficult. Generally, the structure and magnetic properties of thin film systems can be characterized by a variety of methods. Besides techniques like the magneto-optical Kerr-effect (MOKE), ferromagnetic resonance (FMR), vibrating sample and alternating gradient magnetometry (VSM, AGM), or the superconducting quantum interference device (SQUID), x-ray resonant magnetic scattering (XRMS) is particularly very powerful. In XRMS, the resonant absorption of polarized monochromatic synchrotron radiation with an energy of the element specific L- or M-absorption edges leads to a resonant scattering amplitude, which is sensitive to the specific elements' structure and magnetism. Using XRMS, layer thicknesses, interface roughnesses, optical constants, and magnetic behaviour may be characterized. When varying the scattering angle, even a response from a specific depth is possible, which leads to element specific depth profiles of the sample in particular measurement geometries.[10]

Since light-ion bombardment with or without applied field during bombardment changes the magnetic characteristics almost without noticeable structural change,[11] it is tempting to combine XRMS-measurements with light-ion bombardment, where characterization measurements can be performed with very small time delay after bombardment and without breaking the vacuum. To the best of our knowledge, such a combination of technologies is not available to date. Therefore, a plasma ion source has been designed for 5–35 keV He^+ ion bombardment built for combination with an XRMS-diffractometer.

II. ION SOURCE

Main requirements and design parameters for the ion source were: acceleration voltage between 5 keV and 35 keV, fluences between 1×10^{12} and 1×10^{17} ions/cm^2, vacuum of 10^{-6} mbar due to the vacuum requirements at synchrotron radiation sources, and horizontal operation.

A. Overview

The ion source is shown in Fig. 1. It was built with a modular and self-centering optical bench system[12] consisting of circular modules with an outer diameter of 149 mm and of cube elements. The whole ion source must be operable horizontally due to vertically fixed samples in most of the XRMS-diffractometers. Ions are formed in a home-built Penning ion source. After acceleration, an electrostatic einzel lens shapes the beam and provides a focus at the position of the sample in the XRMS-diffractometer. At the central cube, the vacuum

[a]paper@ag-ehresmann.de.

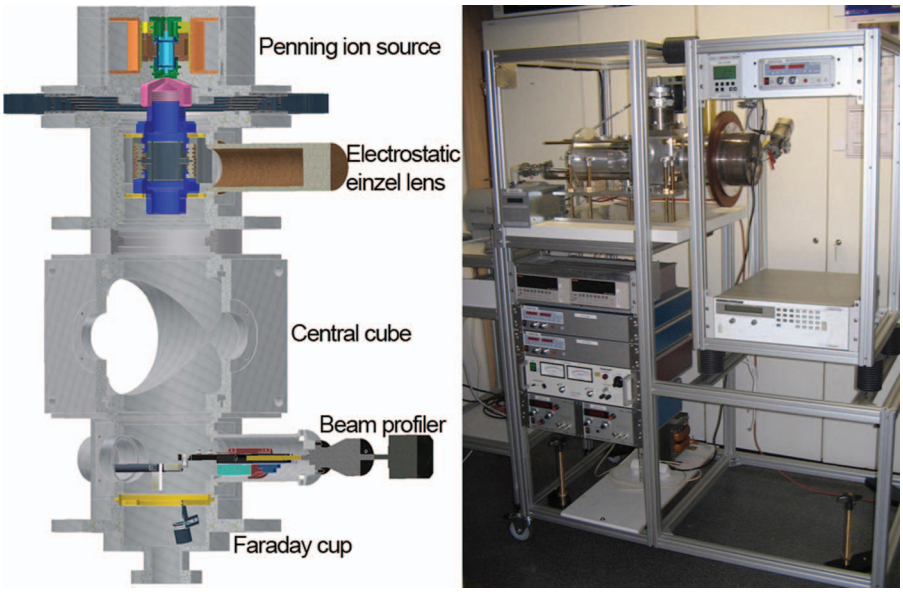

FIG. 1. Schematic setup of the ion gun and photograph of the experimental setup in the transport stage.

pump and a laser based adjustment system was mounted. A beam profiler characterizes the beam profile and a Faraday cup measures the beam current. The components are now described in detail.

B. Penning ion source and acceleration

Briefly, a Penning ion source[13] consists of a plasma volume enclosed by three electrodes with surrounding cooling system, an external magnetic field, an insulating flange, and an extractor aperture. The central electrode is set to high voltage to emit electrons, which are accelerated towards the anode and thereby ionizing the incoming gas atoms. To increase the ionization efficiency, a static external magnetic field forces the electrons on a spiral trajectory extending the electron path in the gas. The plasma volume is encapsulated by a cooling system for thermal stabilization, providing stable plasma conditions in short times. Setting the whole ion source to high voltage, the gas ions are accelerated through a small-sized extractor aperture leading to a diverging ion beam.

In the home-built Penning ion source (Fig. 2(a)), the plasma is ignited in a cylindrical volume (1) with a diameter of 8 mm and a length of 22 mm. To prevent self-excitations, the gas flows into the volume from the side. Electrodes are manufactured from titanium due to its temperature resistivity and resistance against sputtering. The upper and lower electrodes have cavities with a diameter of 4 mm and serve as gas inlet (2) or as extractor aperture (3), simultaneously. Due to its thermal conduction, the cooling component is manufactured from copper including a cooling coil (4), which is operable with different coolants like air, water, or liquid nitrogen. An air coil, made of a coated copper wire and working under standard conditions, provides the external magnetic field, while a plexiglas insulation flange with a thickness of 19 mm prevents leak currents.

With a control system consisting of an EVR 116 control valve and a RVC 300 control unit (both products of *Pfeiffer*), the gas flow from a pressure capsule into the Penning source can be set and controlled at the same time. An *Agilent* dc power supply 654 sets the cathode on high voltage ($\simeq$1 kV), while the magnetic field ($\simeq$1 kOe) is applied by a *HP* 6552A dc power supply. Due to temperature stabilization by ventilation cooling, the plasma and, therewith, the ion beam parameters are stabilized resulting in stable ion currents

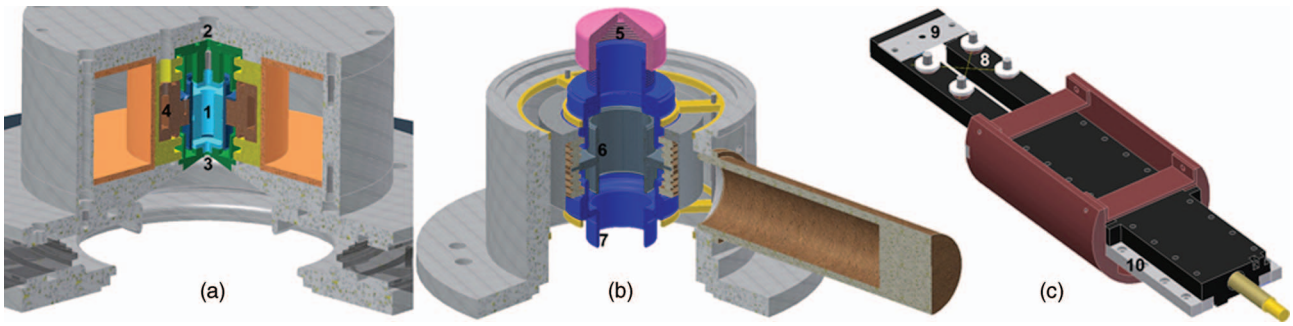

FIG. 2. (a) Schematic setup of the Penning ion source with plasma volume enclosed by three electrodes (1), gas inlet (2), extractor aperture (3), and cooling coil (4). (b) Schematic setup of the Einzel lens with extractor electrode (5), central electrode (6), and lower electrode (7). (c) Schematic setup of the beam profiler with two crossed 20 μm-wires (8), the possibility to mount additional equipment (9), and fixture with adjustment components (10).

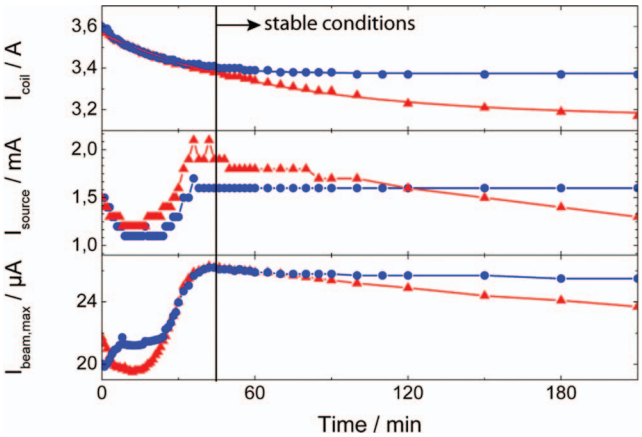

FIG. 3. Time dependence of the currents of the coil I_{coil} delivering the magnetic field, the source I_{source}, and the beam $I_{beam,\,max}$ with (blue circles) and without (red triangles) ventilation cooling.

and beam profiles. Figure 3 indicates that stable conditions are reached 45 min after plasma ignition. By applying a high voltage (5 kV–35 kV) to the Penning source with a *FUG* HCL 140-35500 power supply, the ions are accelerated towards the sample.

C. Electrostatic einzel lens

An electrostatic einzel lens shapes the particle beam and consists of three tubular electrodes in a row. The outer ones are on the same electrostatic potential but differ from the one of the central electrode. The electrostatic fields between two adjacent electrodes cause, in analogy to an optical lens, a focussing or defocussing of the incoming particle beam.

The diverging He^+ ion beam of the ion source enters the einzel lens (Fig. 2(b)) through an aperture of 3 mm diameter, which is on the same potential as the outer electrodes (grounded). A positive high voltage is applied to the central electrode (diameter of 34 mm) generating a convergent einzel lens. To minimize strong edge field effects, all edges of the electrodes are rounded and polished.

The high voltage of the central electrode is applied in the range of 60%–90% of the acceleration voltage (*FUG* HCL 140-35500 power supply). Consequently, the electrostatic einzel lens leads to lower He^+ ion beam divergence (<70%), slight convergence (>80%), or parallel ion trajectories (∼ 75%, see ray tracing of Fig. 4). While the last option is required for ion bombardment over a large area with constant ion fluence, a converging beam allows focussing onto the sample mounted in the diffractometer (distance for most diffractometers between ion source and sample is at least 900 mm) with a spot size down to a few hundreds of micrometer. This option together with additional ion optical elements enables a future ion beam writing when beam blankers are used.

D. Central cube and alignment

For each measurement campaign, the ion source has to be transported to synchrotron radiation facilities and mounted to a diffractometer. This requires high transportability and a

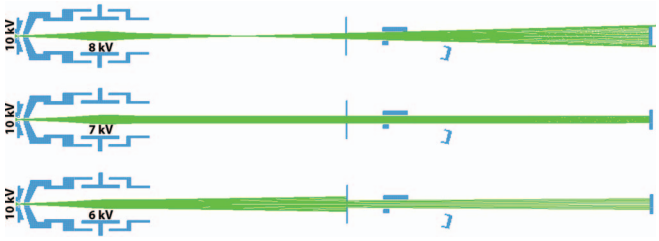

FIG. 4. Simulation of the He^+ ion beam trajectories for different high voltages applied to the Einzel lens central electrode.

quick alignment procedure. Therefore, the recipient and all electronic devices are mounted on 19 inch racks with wheels for transport (see Fig. 1). Four adjustment feet and adjusting screws enable a coarse alignment. The connection to the diffractometer is maintained by flexible bellows at the DN40CF flange, enabling course adjustment of the source with respect to the diffractometer in height and position.

The central cube connects the ion source column with the vacuum pumps and is a universal adapter for the ion beam-sample alignment system and for present and future beam diagnostics. With a turbomolecular pump (200 l/s) backed by a scroll pump, a background pressure of 1×10^{-6} mbar has been achieved within 90 min. The pressure is monitored by a *Pfeiffer* PKR 251 compact full-range gauge.

For fine adjustment, a diode laser is coupled into the recipient through a window of the central cube. The laser beam is deflected by 90° by a pentaprism, which minimizes the sensitivity to slight shifts of the laser position. A linear feedthrough, where the pentaprism is attached, enables an accurate positioning of the laser beam to simulate the ion beam path for sample alignment. To direct the ion beam to the desired position on the sample, the central cube is mounted on two metal plates kept apart by eight adjusting screws. If necessary, the interaction area of the ions with the sample may be set by this alignment system to have a large overlap with the interaction area between sample and synchrotron radiation.

After the alignment, switching times between the two operation modes—ion bombardment and XRMS measurements—totals a few tens of seconds with respect to the motor-driven sample holder, magnet holder, and detector of the diffractometer.

E. Beam profiler

For ion beam profiling, the beam profiler shown in Fig. 2(c) is mounted to the central cube. It contains two crossed wires (diameter: 20 μm) fixed perpendicularly and insulated to each other on a movable stage. The currents induced by the ions in the two wires are measured by two *Keithley* 6485 picoamperemeters. The movement of the stage is performed by a stepping motor from *National Instruments* and the exact position can be determined with a *Renishaw* RGH25Z linear encoder system (0.5 μm resolution). Therewith, it is possible to determine the exact position, the homogeneity, and the total fluence of the ion beam. The profiler stage can be equipped with alternative components for other

types of beam profile measurements, e.g., a sharp blade or apertures for further beam shaping.

F. Faraday cup with beam blanker

The Faraday cup enables ion current measurements close to the sample. It is mounted under an angle of 10° with respect to the ion beam axis, insulated against the recipient, and uses a *Keithley* 6485 picoamperemeter to measure the fluence. A capacitor consisting of two electrodes with different dimensions (see Fig. 1), where the larger electrode is set to high voltage (2 kV) with a *Heinzinger* HCN 3500-40 ump power supply, directs the ion beam into the Faraday cup. When switched off, it does not influence the ion beam.

The ion beam current has to be higher than 1×10^{-8} A through an aperture of 2 mm to implement usual fluences of at least 10^{12} ions/cm^2 in a reasonable time. With the present setup, ion currents of 3×10^{-6} A can be achieved.

III. FIRST EXPERIMENTS

The combined operation of the ion source and of an XRMS diffractometer was tested in first experiments with exchange bias layer systems modified by 10 keV He^+ ion bombardment and characterized by the ALICE diffractometer.[14] Figure 5 shows the schematic setup of the whole recipient. keV He^+ ion bombardment in an external magnetic field changes interfacial coupling and bulk anisotropies due to local delivery of energy into the thin film system and creating defects.[11] These effects enable a tailoring of the unidirectional anisotropy in exchange bias systems. Recently, this technique has been used for a variety of applications, namely in angle sensors,[15] for magnetic logic elements,[16] transport of particles trapped in the stray fields of moving domain walls,[17] mixing small volumes of liquids,[18] controlled movement of domain walls by an external magnetic field,[19] and generating artificial magnetic domain patterns.[20,21]

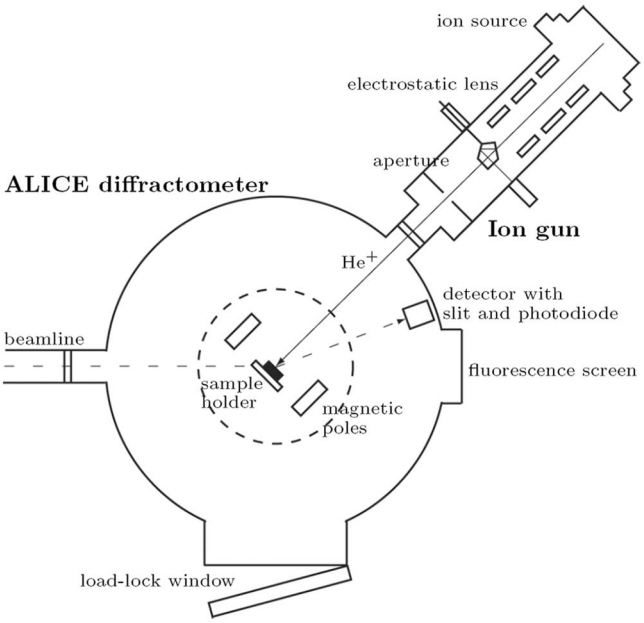

FIG. 5. Schematic setup of the ion gun and the ALICE diffractometer is shown during a bombardment. The He^+ beam (solid line) hits the sample perpendicularly, which has to been moved counterclockwise to measure XRMS (dashed line).

For most of the applications, it is necessary to fabricate layer systems with a temporally stable exchange bias field. However, if keV He^+ ion bombardment is used to tailor the unidirectional anisotropy associated to exchange bias, it was observed that originally stable exchange bias fields in polycrystalline layer systems start to drift after bombardment.[11] This drift was explained by a subtle ion induced change in the distribution of the energy barriers between two minima in the magnetic free energy landscape to be thermally overcome when drifting is observed.[22,23] The experimental method used in the previous investigations were *ex situ* longitudinal magnetooptical Kerr effect (l-MOKE), which averages over a larger area and over the magnetic contributions of different elements when alloys are used in the layer systems. Therefore, as a test experiment for the present combined setup, it will be investigated whether these thermal drifts do influence equally the magnetic moments in both components of an alloyed ferromagnet or whether there are elemental differences in the magnetic behavior of the test system.

[Cu (50 nm)/$Ir_{17}Mn_{83}$ (20 nm)/$Co_{70}Fe_{30}$ (10 nm)/Cu (6 nm)] layer systems with an alloyed CoFe ferromagnet were deposited by rf-sputtering onto a naturally oxidized Si(100) substrate. The exchange bias field was stabilized by field cooling at $T = 300$ °C for $t = 60$ min and was determined to −100 Oe with a coercivity of 31 Oe. Ion bombardment and x-ray scattering experiments were performed at the undulator beamline UE56-PGM2 at BESSY II, Berlin. This beamline enables polarization tuning from linear to circular polarization at photon energies between 60 eV and 1300 eV. This range contains all important L-edges of the investigated layer system. In Bragg-Brentano geometry with an incident angle of $\theta = 8°$, right-handed circularly polarized light with energies of 777.2 eV (Co-L_3-edge), 706.5 eV (Fe-L_3-edge), and 639.0 eV (Mn-L_3-edge) was used to measure the intensity of the reflected light as a function of an applied in-plane magnetic field resulting in element specific hysteresis loops. After magnetic characterization, the layer system was bombarded by different fluences up to 8×10^{13} He^+ ions/cm^2 of 10 keV kinetic energy and at the same time applying an external magnetic field of 1150 Oe antiparallel to the unidirectional anisotropy of the sample (antiparallel bombardment field geometry).

Due to sample, magnet, and detector movement after each bombardment step, the sequential XRMS characterization started 1 min after bombardment. The characterization consisted of single element specific hysteresis measurements with photon energies of the L_3-edges of Co, Fe, and Mn. While each single loop took 1 min, the movement time to set the monochromator to the required L_3-edge energy took 20 s resulting in a total time for one characterization sequence of 4 min (3×80 s). This sequence was repeated once before the sample was stored in remanence and room temperature for 67 min. Then, the sequential measurement was repeated again. All loops have ended at fields where the sample had been in positive magnetic saturation. The first XRMS hysteresis loop of the sample prior to and after He^+ ion bombardment with

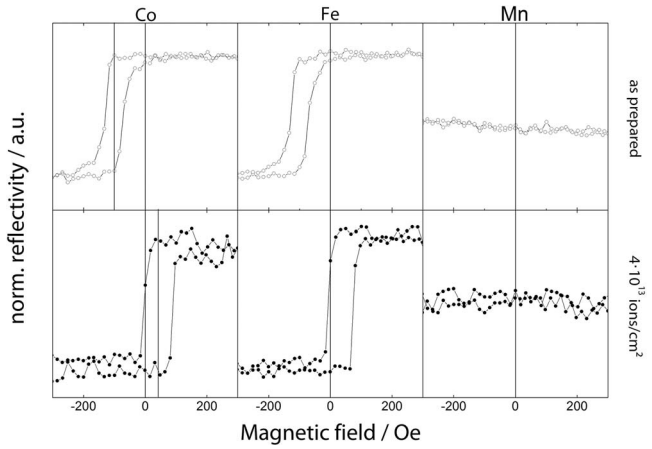

FIG. 6. XRMS hysteresis loops for Co, Fe, and Mn as prepared (open circles) and after He^+ ion bombardment with 4×10^{13} ions/cm^2. Exemplarily, the as prepared ($H_{eb,0}$) and the fluency dependent exchange bias field ($H_{eb}(f)$) is shown for Co.

a fluency of 4×10^{13} ions/cm^2 in antiparallel bombardment field geometry are depicted in Fig. 6. Prior to bombardment, both elements of the alloyed ferromagnets show an exchange bias field of $H_{eb,0} = -100 \pm 2$ Oe, being the same within the experimental uncertainties for both elements. Mn, as a part of the alloyed antiferromagnet, does not display hysteresis. After bombardment, the exchange bias field changed sign similarly for both elements of the ferromagnet while the Mn seems to be still in the antiferromagnetic phase. A fresh sample has then been bombarded by 10 keV He^+ ions in successive fluency steps of 1×10^{13}, 1×10^{13}, 2×10^{13}, and 4×10^{13} ions/cm^2. Figure 7 displays the normalized exchange bias field $H_{eb}(f)/H_{eb,0}$ for the different characterization sequences 1–17. The exchange bias field shift for Co and Fe is the same for both elements within the experimental uncertainties and also the thermal drift after bombardment is the same.

After each bombardment, $H_{eb}(f)$ is decreased and at higher fluences reversed as expected for the antiparallel bombardment field geometry.[24] A surprising result is the thermal drift after bombardment: Whereas past investigations showed and described drifts only towards higher absolute magnitudes of the exchange bias field,[11,22,23] in the present experiments, the drift is observed only towards one direction. This may be explained by one or both of the two major differences of the present measurements to the previous ones: (1) Characterization was performed *in situ* with small time delay between bombardment and characterization; (2) The hysteresis loop of the current sample was not fully shifted to one or the other field side, resulting in two different magnetic states in remanence, which will be set depending on the magnetic history of the sample. Since the storage of the sample has been carried out after the sample has been saturated in the positive direction, the sample is still magnetized in the positive direction in remanence, which may explain this observation. Nevertheless, this finding has to be investigated systematically in future experiments.

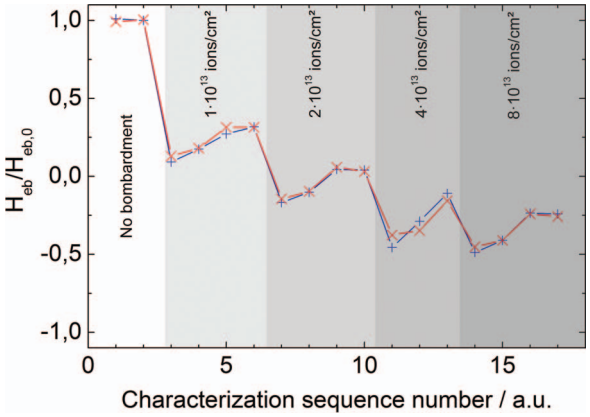

FIG. 7. Exchange bias field for Fe (cross) and Co (plus) normalized to the exchange bias field before bombardment for different ion bombardment fluences.

IV. CONCLUSION

A home-build keV He^+ ion source was designed and built to perform ion bombardment combined with *in situ* element specific XRMS measurements at different synchrotron radiation facilities. The instrument contains a Penning ion source to produce ions, an electrostatic einzel lens for beam shaping, a central cube for an accurate alignment to the sample in the mounted diffractometer, and a stage for measuring and profiling the ion beam precisely. With acceleration voltages up to 30 kV and fluences from 1×10^{12} up to 1×10^{17} ions/cm^2, the ion source yields broad flexibility for different experiments. The setup has been tested at BESSY II, Berlin, showing first element specific measurements of the *in situ* measurements, which suggested the appearance of a so far unobserved relaxation process.

ACKNOWLEDGMENTS

We thank I. Schultz and his colleagues of the Kassel University workshop for the fabrication of most of the components. For using the ALICE diffraction chamber, H. Zabel (Ruhr-University Bochum) is gratefully acknowledged. R. Abrudan helped us to install the source to the ALICE diffractometer and supported us during beamtimes. We also thank F. Radu and B. Zada (Helmholtz-Institut Berlin) for their support with the beamline operation. This work was funded by the project 05KS7RK2 of the German Federal Ministry for Education and Science (BMBF).

[1] G. Carter, V. Vishnyakov, and M. J. Nobes, Nucl. Instrum. Methods Phys. Res. B **115**, 440 (1996).
[2] S. Dhar, T. Kammermeier, A. Ney, L. Pérez, K. H. Ploog, A. Melnikov, and A. D. Wieck, Appl. Phys. Lett. **89**, 062503 (2006).
[3] S. O. Kucheyev, J. S. Williams, C. Jagadish, J. Zou, C. Evans, A. J. Nelson, and A. V. Hamza, Phys. Rev. B **67**, 094115 (2003).
[4] D. Rosenberg and G. K. Wehner, J. Appl. Phys. **33**, 1842 (1962).
[5] D. Ravelosona, C. Chappert, V. Mathet, and H. Bernas, J. Appl. Phys. **87**, 5771 (2000).
[6] J. Ferré, T. Devolder, H. Bernas, J. P. Jamet, V. Repain, M. Bauer, N. Vernier, and C. Chappert, J. Phys. D: Appl. Phys. **36**, 3103–3108 (2003).
[7] P. Kuswik, A. Ehresmann, M. Tekielak, B. Szymanski, I. Sveklo, P. Mazalski, D. Engel, J. Kisielewski, D. Lengemann, M. Urbaniak, C. Schmidt, A. Maziewski, and F. Stobiecki, Nanotechnology **22**, 095302 (2011).

[8]A. Ehresmann, Recent Res. Dev. Appl. Phys. **7**, 401–421 (2004).
[9]J. McCord, T. Gemming, L. Schultz, J. Fassbender, M. O. Liedke, M. Frommberger, and E. Quandt, Appl. Phys. Lett. **86**, 162502 (2005).
[10]J. Geissler, E. Goering, M. Justen, F. Weigand, G. Schütz, J. Langer, D. Schmitz, H. Maletta, and R. Mattheis, Phys. Rev. B **65**, 020405 (2001).
[11]A. Ehresmann, D. Junk, D. Engel, A. Paetzold, and K. Röll, J. Phys. D: Appl. Phys. **38**, 801–806 (2005).
[12]J. Geiger, H. Schmoranzer, H. Jakobs, H. Katterwe, and B. Schröder, Electron Microsc. **1**, 4 (1978).
[13]E. Heinicke and H. Baumann, Nucl. Instrum. Methods **74**, 229 (1969).
[14]J. Grabis, A. Nefedov, and H. Zabel, Rev. Sci. Instrum. **74**, 4048–4051 (2003).
[15]J. Fassbender, S. Poppe, T. Mewes, J. Juraszek, B. Hillebrands, K.-U. Barholz, R. Mattheis, D. Engel, M. Jung, H. Schmoranzer, and A. Ehresmann, Appl. Phys. A **77**, 51–56 (2003).
[16]V. Höink, D. Meyners, J. Schmalhorst, G. Reiss, D. Junk, D. Engel, and A. Ehresmann, Appl. Phys. Lett. **91**, 162505 (2007).
[17]A. Ehresmann, D. Lengemann, T. Weis, A. Albrecht, J. Langfahl-Klabes, F. Göllner, and D. Engel, Adv. Mater. **23**, 5568 (2011).
[18]D. Holzinger, D. Lengemann, F. Göllner, D. Engel, and A. Ehresmann, Appl. Phys. Lett. **100**, 153504 (2012).
[19]M. Urbaniak, P. Kuswik, Z. Kurant, D. Engel, D. Lengemann, B. Szymanski, M. Schmidt, J. Aleksiejew, A. Maziewski, A. Ehresmann, and F. Stobiecki, Phys. Rev. Lett. **105**, 067202 (2010).
[20]A. Mougin, S. Poppe, J. Fassbender, B. Hillebrands, G. Faini, U. Ebels, M. Jung, D. Engel, A. Ehresmann, and H. Schmoranzer, J. Appl. Phys. **809**, 6606–6608 (2001).
[21]J. McCord, R. Schäfer, K. Theis-Bröhl, H. Zabel, J. Schmalhorst, V. Höink, H. Brückl, D. Engel, and A. Ehresmann, J. Appl. Phys. **97**, 10K102 (2005).
[22]A. Ehresmann, C. Schmidt, T. Weis, and D. Engel, J. Appl. Phys. **109**, 023910 (2011).
[23]C. Schmidt, T. Weis, D. Engel, and A. Ehresmann, J. Appl. Phys. **110**, 113911 (2011).
[24]D. Engel, A. Kronenberger, M. Jung, H. Schmoranzer, A. Ehresmann, A. Paetzold, and K. Röll, J. Magn. Magn. Mat. **263**, 275–281 (2003).